# Modified Chitosan Immobilized on Modified Sand for Industrial Wastewater Treatment in Multicomponent Sorption: Shrimp Biowaste Processing

Hamza El Fargani[1] Rajae Lakhmiri[1*] Hammadi El Farissi[1] Abdallah Albourine[2] Mohamed Safi[3] Omar Cherkaoui[4]

1. Laboratory of Materials and Valorization of the Resources, Faculty of Sciences and Techniques of Tangier, Abdelmalek Essaâdi University, Km 10 route de Ziaten, BP 416 Tangier, Morocco
2. Laboratory of Materials and Environment, Team of Coordination Chemistry, Faculty of Sciences, Ibn Zohr University ,BP 8106, 80000 Agadir, Morocco
3. Laboratory of Physical Chemistry and Bio-Organic Chemistry, Faculty of Sciences and Techniques- Mohammedia, URAC 22 University of Hassan II Mohammedia- Casablanca, , BP 146,Mohammedia, Morocco
4. Laboratory REMTEX, Higher School of Textile and Clothing Industries, Casablanca, Morocco

* E-mail of the corresponding author: lakhmirir@yahoo.fr

## Abstract

In this paper, modified chitosan immobilized on modified sand (MCs/MS) was synthesized and characterized by infrared spectroscopy (FT-IR), X-ray diffraction (XRD), scanning electron microscope (SEM) and energy dispersive X-ray analysis (EDXA). MCs/MS composite was used to remove Reactive Red 23 (RR23), Reactive Blue 19 (RB19) and Iron III ($Fe^{3+}$) in three single-component and three binary, RR23+RB19, RR23+$Fe^{3+}$ and RB19+$Fe^{3+}$. Batch experiments were carried out for adsorption kinetics, isotherms and thermodynamics. Operational parameters studied were pH, contact time, temperature, adsorbate and adsorbent concentrations. Adsorption kinetics in single and binary systems of components followed pseudo- second-order kinetics model. The isotherm data in single and binary systems followed Freundlich isotherm model. Thermodynamic parameters have disclosed that the adsorption is exothermic and not spontaneous with a physical adsorption for both single and binary systems. The results showed that MCs/MS composite was an effective adsorbent to remove hazardous pollutants with a removal rate between 80% and 99.6%, the optimal contact time was between 120 and 180 min for all components in single and multicomponent system.

**Keywords :** Modified chitosan immobilized on modified sand, Multicomponent system, Reactive Red 23, Reactive Blue 19, Iron III, Hydrothermo-Chemical method.

## 1. Introduction

Effluents that contain significant amount of toxic metals and dyes are generated by industrial sources such as dyestuffs, textile, paper, plastics, automotive and metal fabrication. Metals and dyes can be toxic pollutants that are non-biodegradable, undergo transformations, and have great environmental, public health, and economic impacts [1]. Iron plays an essential role in photosynthesis and is the limiting growth nutrient for phytoplanktons in some parts of the ocean [2] and for human health too. However, intake of Iron (III) at high dosages can cause health problems and they become toxic at higher levels [3]. It is, therefore, important to remove any excess amount of Iron present in wastewater in order to protect the public health and to prevent pollution of the surface water and groundwater [4]. In the other hand, there are over 100.000 commercially available dyes and more than $7 \times 10^5$ tones are produced annually [5,6]. The removal of dyes from waste effluents becomes environmentally important because even a small quantity of dye in water can be toxic and highly visible [7,8], real textile wastewater is a mixture of dyes, organic compounds, heavy metals, dissolved solids, surfactants, salts, and chlorinated compounds [9], the purpose of our study is to reflect the industrial reality by working on multicomponent systems containing dyes and metals.

Conventional technologies that treat metals and dyes effluents are membrane separation, electrodeposition, ion exchange, chemical precipitation, and solvent extraction. There are several disadvantages such as high

operating cost and inefficiency in removing trace quantities of metals and dyes from waste streams. Another disadvantage is the production of sludge or mud, which requires proper disposal and confinement [10]. On the contrary, adsorption is an effective and economical method among the physicochemical treatments [11].

Chitosan (Cs), a naturally occurring linear polymer of glucosamine has exhibited excellent adsorption capacity for anionic dyes and metal ions and great modification capability because chitosan molecules contain a large number of active amine ($-NH_2$) groups [12]. Sand (S) is a low-cost material and also very abundant in nature wildly used in water treatment. Embedding chitosan with sand can provide physical support and increase the accessibility of binding sites. In order to ameliorate the efficiency of our adsorbent, physical and chemical modification needs to be carried out on chitosan and sand, physical modification reduces the crystalline state of sand and chitosan witch results in an expansion of the polymer network that allows an easy access to its binding sites [13]. On the other hand, chemical modification enhances mechanical strength, improves chemical stability in acidic and alkaline medium, and increases the resistance to microbiological and biochemical degradation [14-16]. The aim of this study is to investigate the adsorption behavior of modified chitosan immobilized on modified sand (MCs/MS) toward RR23, RB19 and $Fe^{3+}$ in single and multicomponent systems.

## 2. Materials and methods

### 2.1. Analytical instruments

Infra-red spectrophotometer (FT-IR) of type JASCO FT/IR-410 on potassium bromide pastilles KBr with 2% of MCs/MS composite is used to characterize our product and defined the functional groups, The obtained spectrum was recorded between 4000 $cm^{-1}$ and 400 $cm^{-1}$. To define our composite structure we used the X-ray diffraction (XRD) type Brukker D8 Advance ECO. The surface morphology, the adsorbent elements localization and the qualitative detection were given by the Scanning Electron Microscope (SEM) supplied with energy dispersive X-ray analysis (EDXA).

The adsorbed quantities measurements of Reactive Red 23 (RR23), Reactive Blue 19 (RB19) and Iron (III) ion formerly called ferric ($Fe^{3+}$) on our composite were carried out in an analysis wavelength $\lambda_{max}$: 511 nm, $\lambda_{max}$: 592 nm and $\lambda_{max}$: 510 nm [17], respectively, on a spectrophotometer UV of the type JASCO V-360 with a preliminary calibration of the instrument spectrophotometer to detect the parameters affect on the adsorption process in single and multicomponent systems.

### 2.2. Materials

The sand samples were taken from the shallow waters of Larache city beach, Morocco. Chitosan with a deacetylation degree of 85% was extracted by Hydrothermo-Chemical way [12] starting from Scandinavian prawns. Sodium hydroxide NaOH, hydrochloric acid HCL, Sulfuric acid $H_2SO_4$ and epichlorohydrin (ECH) were from Sigma-Aldrich and all other chemicals used were of analytical quality.

### 2.3. Methods

#### 2.3.1. Hydrothermo-Chemical method for the extraction of chitosan

The Hydrothermo-Chemical method [12] followed to the chitosan extraction based on two parts a demineralization in acidic medium HCl 2M for 2.5 h at a temperature of 50 °C and a simultaneous deproteination/desacetylation in basic medium NaOH 12.5M for 2 h at a temperature of 110 °C with a solid/liquid ratio of 1:10 (dry carapace weight/volume of diluted solution).

#### 2.3.2. Sand Modification

The sand samples were taken from the shallow waters of Larache city beach, Morocco. The sand samples were thoroughly washed to remove all impurities then dried in the drying oven at 105 °C overnight. After drying, the particles size of the sand samples was maintained (200 μm) by using various sieves. The sand was modified by soaking in 40% $H_2SO_4$ for 4 hours, then the treated sample was washed several times with distilled water and finally drying the modified sand in the drying oven at 105 °C overnight [18].

### 2.3.3. Chitosan immobilized on modified sand preparation

About 5 g of chitosan and 100 g of modified sand are stirred in 300 ml of HCl 5% (v/v) for 5 h. NaOH of 1M were added by degrees until neutralization occurred, after adsorbent stabilization, we washed with distilled water and finally dried for 24 hours in the drying oven at a temperature of 65 °C [19-21].

### 2.3.4. Modified chitosan immobilized on modified sand synthesis

Epichlorohydrin solution 0.10 M containing sodium hydroxide 0.067 M was prepared (pH 10). Chitosan immobilized on modified sand freshly prepared was added to the epichlorohydrin solution (ECH) to obtain a 1:1 molar ratio with chitosan (Cs) (ECH mole: mole Cs) with heating at a temperature between 40 and 50 °C under continuous stirring with a magnetic stirrer for 2 h. The composite was intensively washed through a 200 µm sieve with distilled water to remove any epichlorohydrin which has not reacted and any residual NaOH, HCl or $H_2SO_4$, finally dried at a temperature of 65 °C for 24 hours in the drying oven [22].

### 2.3.5. Adsorption procedure

Different amounts of MCs/MS composite from 10mg to 260mg were mixed with the components RR23, RB19 and $Fe^{3+}$ in single (Sin) and binary (Bin) systems in Erlenmeyer flasks containing 30 ml of component solution at neutral pH in ambient temperature, initial component concentration of 50 mg/l under stirring at 150 rpm for 90 min to studied the effect of the adsorbent dose.

The pH of the solution was adjusted from 1 to 11 by using NaOH and HCL with an adsorbent mass of 70 mg, initial component concentration of 50 mg/l, in ambient temperature under continuous stirring at150 rpm for 90 min to study the optimal pH which gives the maximum adsorption capacity in both single and multicomponent systems. Distilled water was used to prepare all components solutions to preclude and underplay possible interferences in this study.

The calculation of the amount adsorbed ($q_e$) and the removal percentage (R%) of the three components were carried out by equations (1) and (2):

$$\text{Amount adsorbed}(q_e) \frac{C_0 - C_e}{M} * V \quad (1)$$

$$\text{Removal}(\%) = \frac{C_0 - C_e}{C_0} * 100 \quad (2)$$

Where $C_0$ is the initial dye concentration in solution (mg/l), $C_e$ is the final dye concentration in solution (mg/l), M is the adsorbent mass (g) and V is the solution volume.

Various component concentrations were used to conduct the adsorption experiments employing 70 mg of composite for RR 23, RB 19 and $Fe^{3+}$ in single and binary systems with a neutral pH in ambient temperature for 90 min under continuous stirring at 150 rpm to attain equilibrium conditions (Table 1).

Table1. Initial components concentrations used in single and binary systems.

| Single system | | | Binary system | | |
|---|---|---|---|---|---|
| $C_0$ (mg/l), RR23(Sin) | $C_0$ (mg/l), RB19(Sin) | $C_0$(mg/l), Fe3+(Sin) | $C_0$ (mg/l), RR23(Bin) | $C_0$ (mg/l), RB19(Bin) | $C_0$(mg/l), $Fe^{3+}$ (Bin) |
| 10 | 10 | 10 | 5 | 5 | 5 |
| 25 | 25 | 25 | 12.5 | 12.5 | 12.5 |
| 50 | 50 | 50 | 25 | 25 | 25 |
| 100 | 100 | 100 | 50 | 50 | 50 |
| 150 | 150 | 150 | 75 | 75 | 75 |
| 200 | 200 | 200 | 100 | 100 | 100 |
| 250 | 250 | 250 | 125 | 125 | 125 |
| 300 | 300 | 300 | 150 | 150 | 150 |

The calculation of the components concentrations in the binary systems [23] were proceeded by the equations (3) and (4). For a binary system of components A and B, measured at $\lambda_1$ and $\lambda_2$, respectively, to obtain optical densities of $d_1$ and $d_2$ [24,25]:

$$C_A = (k_{B2}d_1 - k_{B1}d_2) / (k_{A1}k_{B2} - k_{A2}k_{B1}) \quad (3)$$

$$C_B = (k_{A1}d_2 - k_{A2}d_1) / (k_{A1}k_{B2} - k_{A2}k_{B1}) \quad (4)$$

Where $C_A$ and $C_B$ are the concentrations of components A and B in binary systems, respectively. $k_{A1}$, $k_{B1}$, $k_{A2}$, and $k_{B2}$ are the calibration constants for components A and B at the two wavelengths of $\lambda_1$ and $\lambda_2$, respectively. The calibration constants for the three components at three different wavelengths are shown in Table 2.

Table2. Calibration constants values for the calculations of component concentration in the mixtures starting from the optical density values.

| Component name | $\lambda$/nm | Calibration constants | | |
|:---:|:---:|:---:|:---:|:---:|
| **RR23** | $\lambda_1$ <br> 511 | $K_{RR1}$ <br> 0.1153 | $K_{RR2}$ <br> 0.0034 | $K_{RR3}$ <br> 0.1149 |
| **RB19** | $\lambda_2$ <br> 592 | $K_{RB1}$ <br> 0.0189 | $K_{RB2}$ <br> 0.0441 | $K_{RB3}$ <br> 0.0293 |
| **Fe$^{3+}$** | $\lambda_3$ <br> 510 | $K_{Fe1}$ <br> 0.0022 | $K_{Fe2}$ <br> 0.0004 | $K_{Fe3}$ <br> 0.0008 |

To establish the adsorption kinetics during the adsorption process, the absorbance variations were given at different time intervals between 10min to 300min with an adsorbent mass of 70 mg, initial component concentration of 50mg/l, pH 7 with a continuous stirring at 150 rpm in ambient temperature.

The effect of the temperature on adsorption was carried out with different temperatures at 25 ℃, 45 ℃, 65 ℃ and 85 ℃ under following conditions: adsorbent mass of 70 mg with an initial component concentration of 50 mg/l under continuous stirring at 150 rpm for 90 min. After the experiments, the samples were centrifuged by a centrifugal machine of the type P.SELECTA Mixtasel, and then the component concentrations were given for both systems.

To describe the adsorption phenomenon it's necessary to use different isotherm models like Freundlich, Langmuir, Temkin and Dubinin-Radushkevich and various kinetic models as pseudo-first-order, pseudo-second-order, the intraparticle diffusion and the Elovich model. The determination of thermodynamic parameters gives us a clear idea about our adsorption process.

## 3. Results and discussion

### 3.1. Modified Chitosan/Modified Sand composite (MCs/MS) Characterization

FT-IR spectroscopy was used to characterize chitosan (Cs), sand (S), modified sand (MS) and modified chitosan/modified sand composite (MCs/MS) to confirm the immobilization of modified chitosan on modified sand surface. Figure 1 presents the infrared spectra of Cs, S, MS and MCs/MS composite. The chitosan (Cs) contains characteristic bands at 3436 cm$^{-1}$ (-OH and -NH$_2$ stretching vibrations), 2930 cm$^{-1}$ (-CH stretching vibration in -CH and -CH$_2$), 1659 cm$^{-1}$ (-NH$_2$ bending vibration), 1379 cm$^{-1}$ (-CH symmetric bending vibrations in -CHOH), 1076 cm$^{-1}$ and 1026 cm$^{-1}$ (-CO stretching vibration in -CONH), sand (S) main bands can be assigned as follows: 3400 cm$^{-1}$ (strong and broad stretching vibration band of -OH associated with alcohols and phenols), 2872 cm$^{-1}$ (strong asymmetric stretching vibration band of C-H bond of the alkane groups), 2132 cm$^{-1}$ (weak stretching band of the alkyne groups), 1794 cm$^{-1}$ (strong stretching band of the acid group -C=O), 871 cm$^{-1}$ (stretching vibration of Si-O) [26] and 692cm$^{-1}$ (twisting vibration of Si-O-Si) [26]. The FT-IR spectrum of S and MS differs at two bands 3608cm$^{-1}$ (variable and thin stretching band of free O-H bond of alcohols and phenols) and 3548cm$^{-1}$ (intense stretching band of O-H bond of the acid group) due to modification with the strong acid H$_2$SO$_4$.

The main bands of the MCs/MS composite (Figure 1, (d)) are 3445cm$^{-1}$, 2876cm$^{-1}$, 2130cm$^{-1}$, 1794cm$^{-1}$, 1103cm$^{-1}$, 874cm$^{-1}$ and 694 cm$^{-1}$ are assigned to stretching vibration band of the N-H bond of the primary and secondary amine groups, a symmetrical stretching average band of the C-H bond of the alkane groups, stretching band of the alkyne groups, strong stretching band of the C=O bond of the acid group, strong asymmetric stretching band of the (C-)$_2$O bond of epichlorohydrin during treatment of chitosan [27], Si-O stretching vibration and Si-O-Si twisting vibration [26].
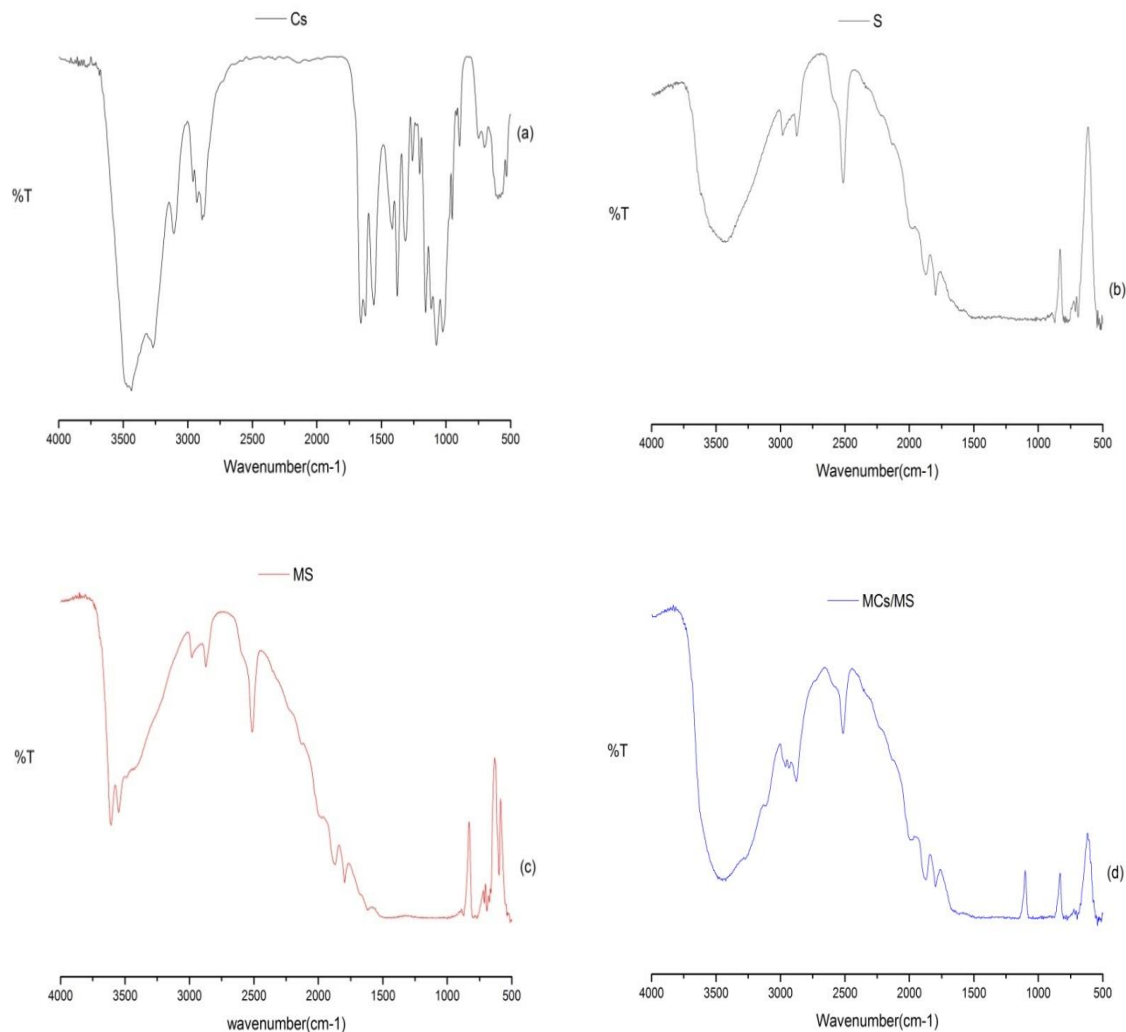
Figure 1. FTIR spectra of the Cs (a), S (b), MS (c) & MCs/MS (d).

Figure 2 shows the X-Ray diffractograms of Cs, S, MS and MCs/MS composite. The chitosan (Cs) shows characteristic peaks in $2\theta=9.2°$; $12.5°$; $19.8°$; $26.03°$ and $39.4°$ that caused by diffraction from (010) and (100) planes and (020) planes of the crystalline lattice [28]. The sand (S) EDX has characteristic peaks in $2\theta=21°$; $26.8°$; $29.6°$; $40.5°$ and $42.8°$ which represent the crystalline structure of quartz, it is clear that silica ($SiO_2$) represents the major component with calcium (Ca). Based on the characteristic peaks treatment of modified sand (MS) $2\theta=21°$; $26.8°$; $36.7°$ and $42.5°$ which agree with the crystalline structure of quartz and silvialite ($Ca_4Al_6Si_6O_{24}(SO_4)$) due to the modification with sulfuric acid $H_2SO_4$.

The X-Ray diffractogram of MCs/MS composite (Figure 2, (d)) shows characteristic peaks in $2\theta=21°$; $26.8°$; $39.7°$; $42.7°$ and $46°$ corresponds to the crystalline structure of quartz and carbon nitride (CN), which gives very important properties to our composite such as mechanical and chemical stability [29].
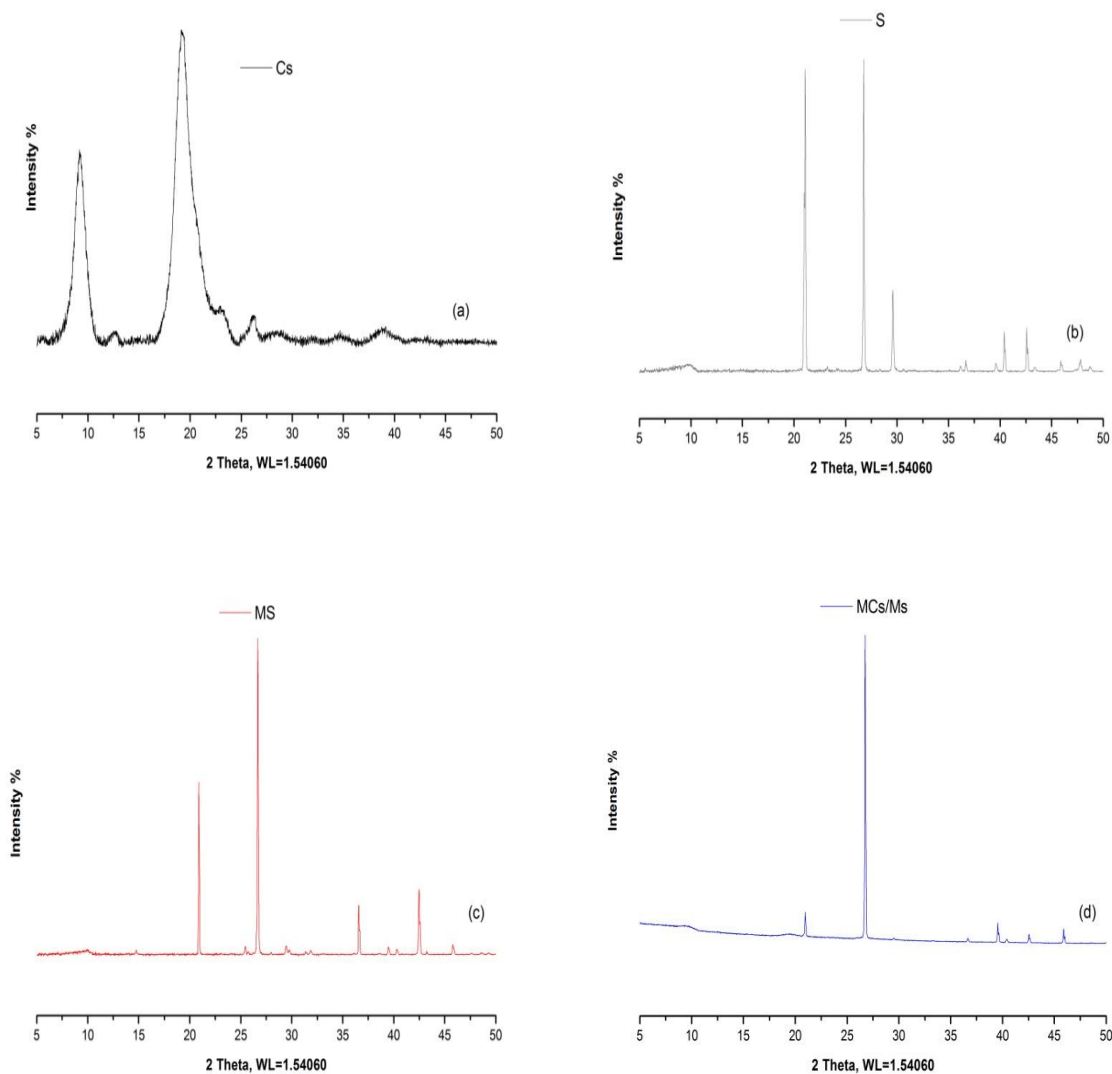
Figure 2. X-ray diffractograms of the Cs (a), S (b), MS (c) & MCs/MS (d).

Figure 3 represents the SEM micrographs of chitosan (a), sand (b), modified sand (c), and modified chitosan/modified sand (MCs/MS) composite (d). According to the SEM micrographs we can perceive a smooth morphology for both chitosan (a) and sand (b), in contrast on the modified sand (c) one notices a porous structure due to modification with the strong acid $H_2SO_4$.

The modified chitosan/modified sand (MCs/MS) composite (Figure 3, (d)) micrograph shows that a large number of surface pores are unsmooth with a porous structure, the presence of porous chitosan tied to the surface evince that modified chitosan is effectively immobilized on modified sand surface.

The quantitative elemental composition of chitosan (a), sand (b), modified sand (c) and modified chitosan/modified sand composite (d) are indicated in Figure 4. MCs/MS composite EDXA diffractogram proved the presence of elements such as carbon, oxygen, nitrogen, silicon, calcium and aluminum in the composite.
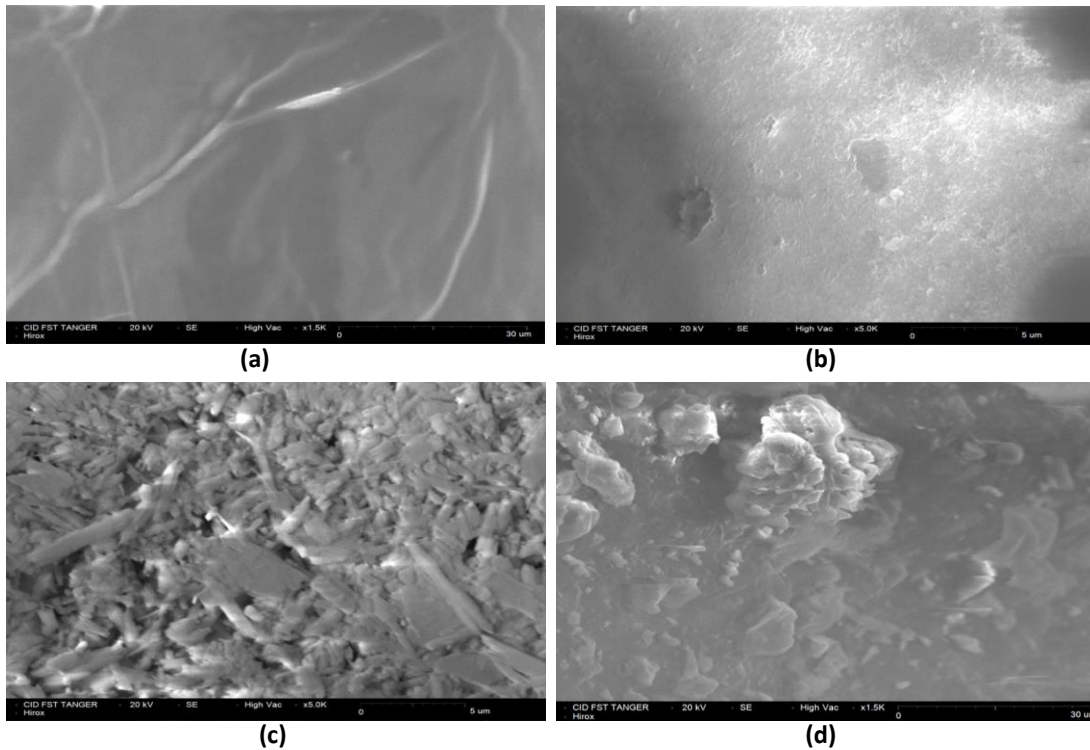
Figure 3. SEM micrographs of chitosan (a), sand (b), modified sand (c),
and modified chitosan/modified sand (d).
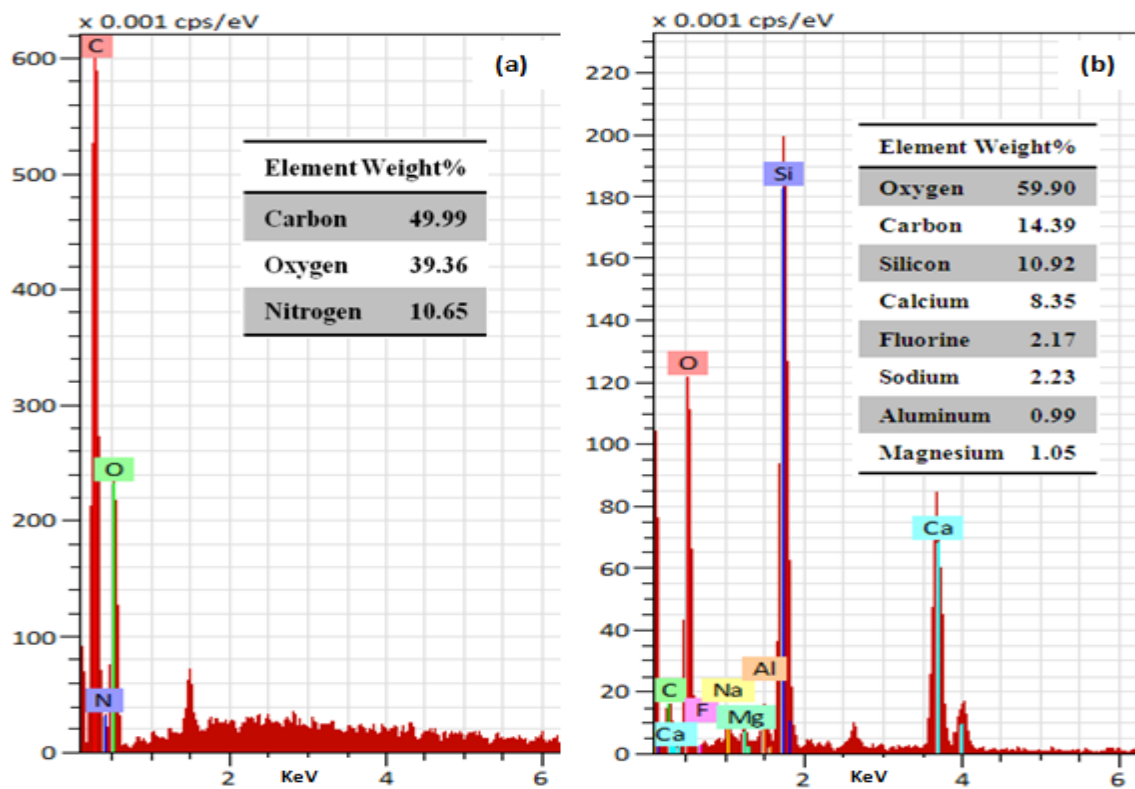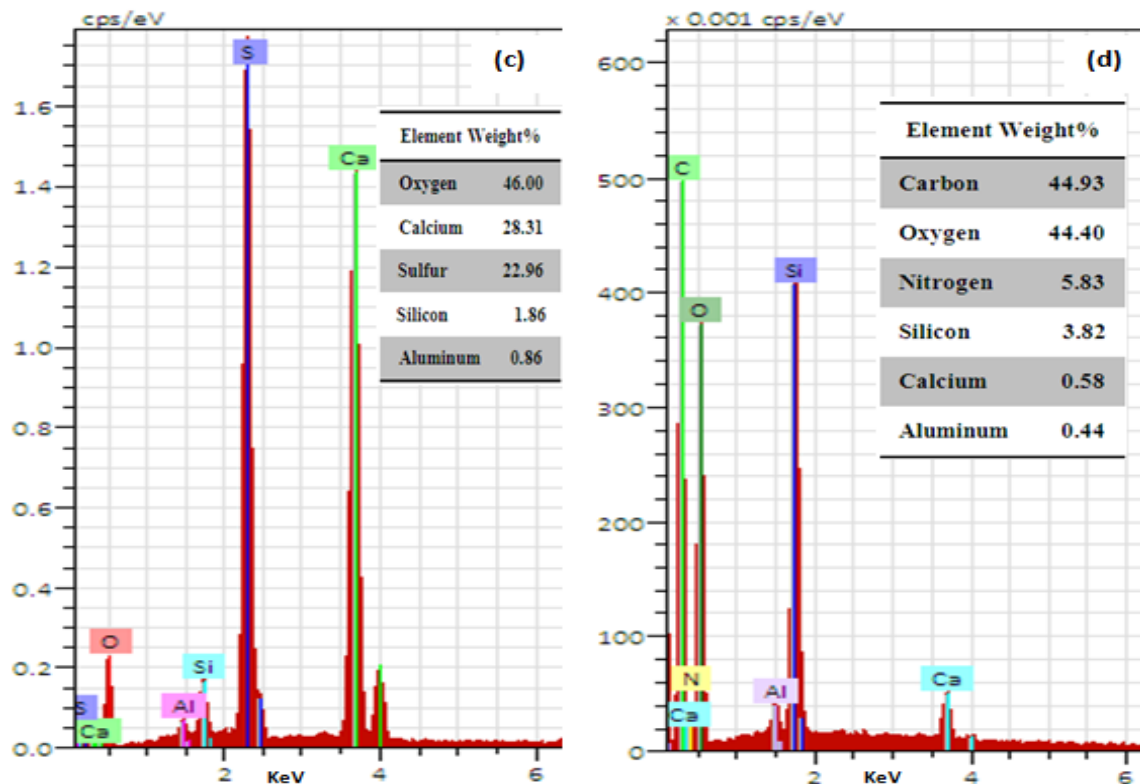
Figure 4. EDXA diffractograms of chitosan (a), sand (b), modified sand (c), and modified chitosan/modified sand composite (d).

### 3.2. Effect of operational parameters on components removal

### 3.2.1. Effect of adsorbent dose

The study of the adsorbent dose on the adsorption process of RR23, RB19 and $Fe^{3+}$ in single (Sin) and binary (Bin) systems was performed in erlenmeyers containing 30 ml of components solution with neutral pH in ambient temperature under stirring at 150 rpm with an initial component concentration of 50mg/l during 90 min. Different amounts of composite from 10mg to 260mg were used for RR23, RB19 and $Fe^{3+}$ in both systems. The samples were centrifuged after balance and the component concentration in the supernatant solution was examined.

Figure 5 demonstrates the effect of adsorbent dose on the components removal from single and binary systems of components. The removal rate (R%) of components rises up with rising the adsorbent dose to a specific boundary to attain a fixed value, the optimal adsorbent amounts for the removal of RR23, RB19 and $Fe^{3+}$ in single and binary systems are given in Table 3.

When the adsorbent dose is increased it is observed that the removal rate also increases, that can be attributed to the availability of several adsorption sites and the increase in the adsorbent surface area. From Figure 5 and Table 3 we can notice that binary systems containing $Fe^{3+}$ as one of the components represents a higher retention rate R%  than the binary system containing only dyes, this can be attributed to the presence of two adsorption mechanisms, the electrostatic interaction due to the availability of several positively charged active sites used only for the adsorption of the anionic dyes and the chelating mechanism for the cationic metals $Fe^{3+}$ fixation, in other words there is less competition on the active adsorption sites between the two components.
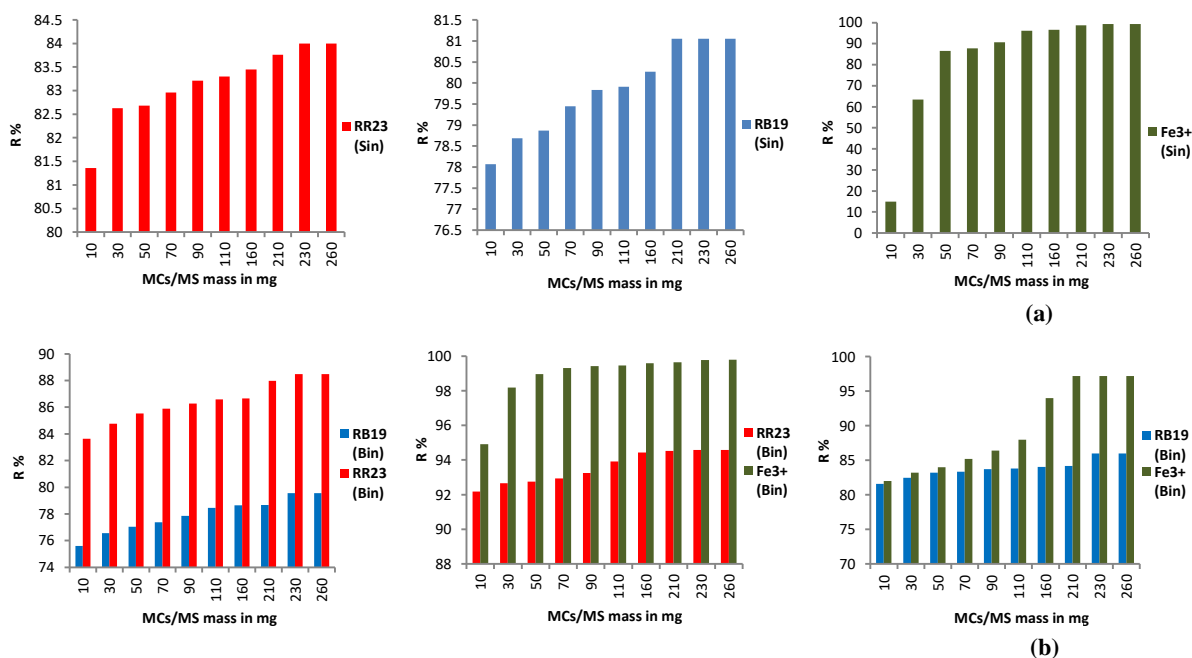
Figure 5. Effect of MCs/MS amount on the adsorption of components RR23, RB19 and $Fe^{3+}$ in single (a) and binary (b) systems of components. (Time=90min, Initial component concentration=50mg/l, Stirring=150rpm, Ambient temperature and pH~7)

Table 3. Optimal adsorbent amounts for the removal of components RR23, RB19 and $Fe^{3+}$ in single (Sin) and binary (Bin) systems.

| System | | Optimal adsorbent amount in mg | R% |
|---|---|---|---|
| **Single** | **RR23** | 210 | 83.7 |
| | **RB19** | 160 | 80 |
| | **$Fe^{3+}$** | 210 | 98.6 |
| **Binary** | **RR23+RB19** | | |
| | **RR23** | 210 | 87.9 |
| | **RB19** | 210 | 78.6 |
| | **RR23+$Fe^{3+}$** | | |
| | **RR23** | 210 | 94.5 |
| | **$Fe^{3+}$** | 210 | 99.6 |
| | **RB19+$Fe^{3+}$** | | |
| | **RB19** | 210 | 84.2 |
| | **$Fe^{3+}$** | 160 | 94 |

### 3.2.2. Effect of pH

The aqueous solution pH plays a significant role onto the surface of MCs/MS composite during the adsorption. The modified chitosan attached to the modified sand surface contains amine groups, $-NH_2$, which is readily protonated to form an $-NH_3^+$ groups, in acidic solutions. The pH solution can also influence the various composite functional groups such as hydroxyl groups, carbonyl groups and amine groups of modified chitosan which represents the main active groups during the adsorption for both single and binary systems of components. The effect of pH on the RR23, RB19 and $Fe^{3+}$ adsorption in single and binary systems of components by the MCs/MS composite is shown in Figure 6. Maximum components adsorption occurred at pH1.

The metals complexity by chitosan can involve two different mechanisms: chelation and ion exchange depending on the solution composition, the metal ions type and pH. This latter parameter may affect the macromolecule protonation. At pH 1, a remarkably high electrostatic attraction exists between the positively

charged adsorbent surface, due to the ionization of the adsorbent functional groups and the negatively charged anionic dyes. Thus, it makes it possible to promote the chelation mechanism for the cationic metals $Fe^{3+}$ fixation. The amine groups are the main reactive groups for the metal ions although the hydroxyl groups, particularly at the C-3 position, can contribute to the adsorption in both single and binary systems.
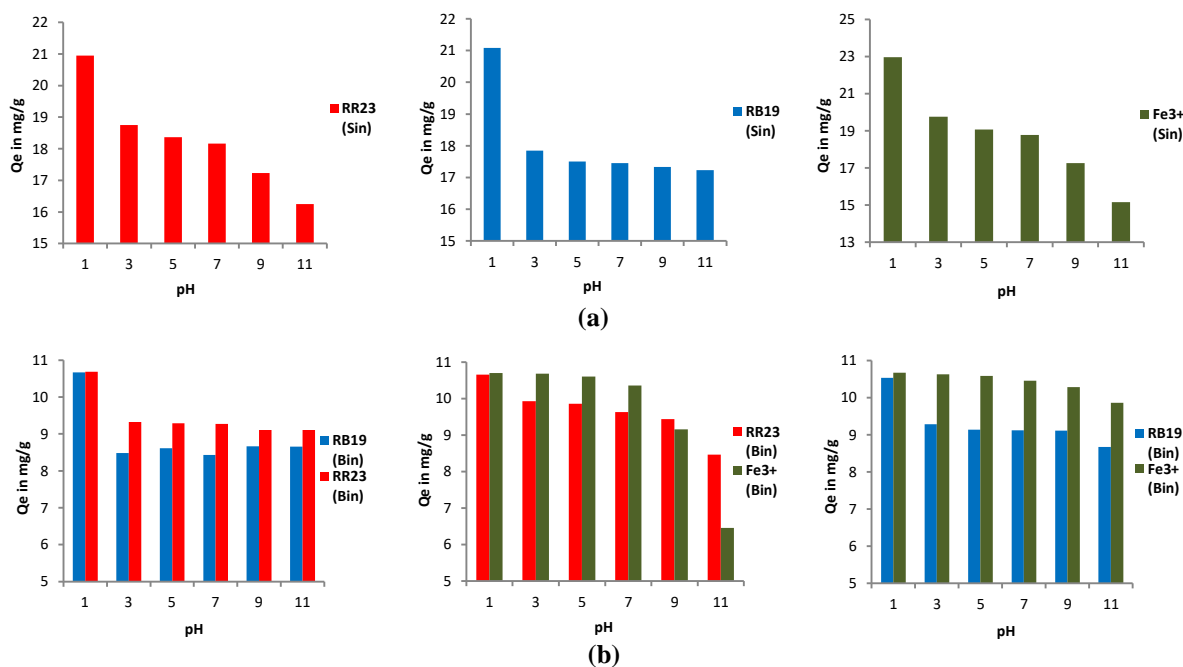


Figure 6. Effect of pH on the RR23, RB19 and $Fe^{3+}$ adsorption on the MCs/MS composite in single (a) and binary (b) systems. (Time=90min, Ambient temperature, Initial component concentration=50mg/l, Adsorbent mass=70mg, Stirring=150rpm).

### 3.2.3. Effect of Initial component concentration

The study of the effect of initial components concentration in both systems was carried out with MCs/MS composite mass of 70mg added to 30ml of RR23, RB19 and $Fe^{3+}$ in single and binary systems at different component concentrations from 10mg/l to 300mg/l (Table 1) at a neutral pH in ambient temperature for 90 min under continuous stirring at 150 rpm. The adsorption capacity rises up with the rising of the initial components concentration for both systems until balance as indicated in Figure 7 and Figure 8, the main cause is the elevation of the motive force of the concentration gradient.
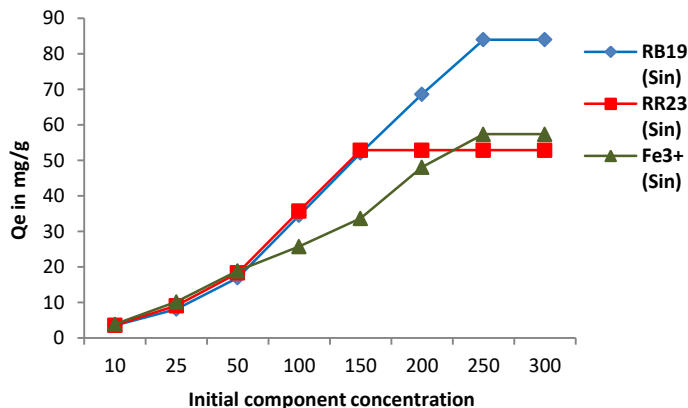


Figure 7. Effect of the initial component concentration on the adsorption of RR23, RB19 and $Fe^{3+}$ in the single system (Sin) (Time=90 min, Ambient temperature, Adsorbent mass=70 mg, Stirring=150 rpm and pH~7)
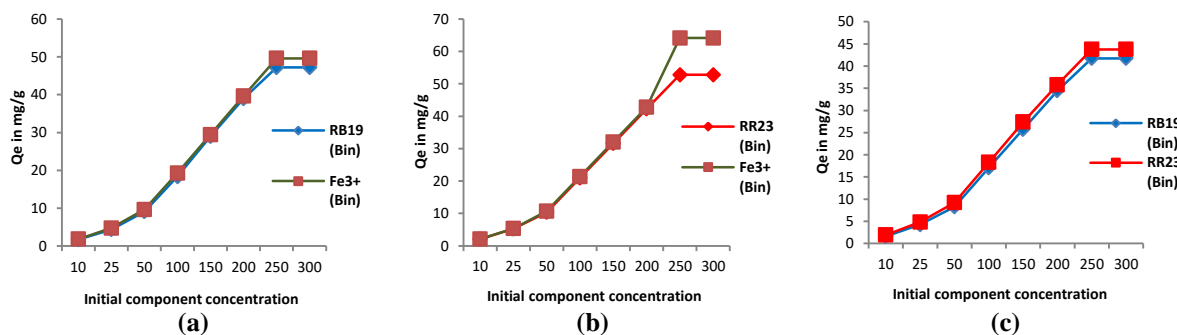
Figure 8. Effect of the initial component concentration on the adsorption of RR23+RB19 (a), RR23+Fe$^{3+}$ (b) and RB19 + Fe$^{3+}$ (c) in the binary system (Bin). (Time=90 min, Ambient temperature, Adsorbent mass=70 mg, Stirring=150 rpm and pH~7)

According to Figures 7 and 8 we can notice that the optimal initial components concentrations are obtained only from the bearing, Table 4 shows the optimal initial components concentrations in single and binary systems.

Table 4. Optimal initial concentrations of components RR23, RB19 and Fe$^{3+}$ in single and binary systems. (Time=90 min, Ambient temperature, Adsorbent mass=70 mg, Stirring=150 rpm and pH~7)

| System | | Optimal initial concentration in mg/l | Qe in mg/g |
|---|---|---|---|
| **Single** | **RR23** | 100 | 35.7 |
| | **RB19** | 200 | 68.5 |
| | **Fe$^{3+}$** | 200 | 48 |
| **Binary** | **RR23+RB19** | | |
| | **RR23** | 200 | 35.7 |
| | **RB19** | 200 | 34.4 |
| | **RR23+Fe$^{3+}$** | | |
| | **RR23** | 200 | 42.2 |
| | **Fe$^{3+}$** | 200 | 42.7 |
| | **RB19+Fe$^{3+}$** | | |
| | **RB19** | 200 | 38.9 |
| | **Fe$^{3+}$** | 200 | 39.6 |

From all these results, we can conclude that the optimal initial concentration of the components RR23, RB19 and Fe$^{3+}$ to achieve the equilibrium adsorption capacity is 200mg/l for both single and binary systems of components.

### 3.2.4. Effect of contact time

The effect of contact time on the adsorption is fundamental to define the contact time relating to the adsorption equilibrium. Both Figures 9 and 10 illustrates the adsorption capacity evolution of components RR23, RB19 and Fe$^{3+}$ in single and binary systems based on liquid/solid contact time.

The findings obtained prove that the adsorption capacity increases with the increase in contact time until balance, the optimal contact time is between 120 min and 180 min for the RR23, RB19 and Fe$^{3+}$ in both single and binary systems of components. Table 5 represents the liquid/solid contact time for components RR23, RB19 and Fe$^{3+}$ in single and binary systems of components with the various equilibrium adsorption capacities Qe.
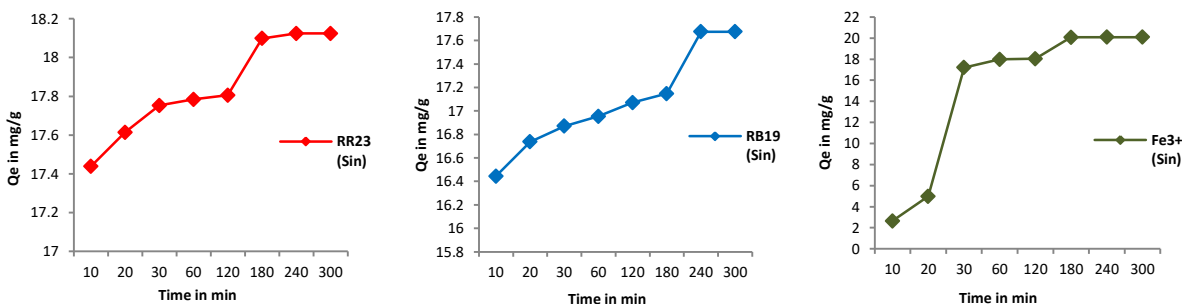
Figure 9. Effect of contact time on the adsorption of components RR23, RB19 and $Fe^{3+}$ on the MCs/MS composite in the single system (Sin). (Ambient temperature, Adsorbent mass=70 mg, Initial component concentration=50 mg/l, Stirring=150 rpm and pH~7)



**(a)** **(b)** **(c)**
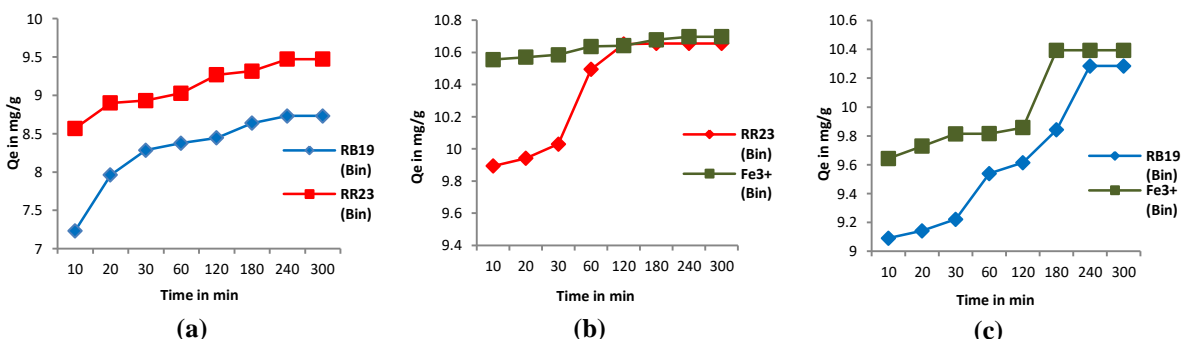
Figure 10. Effect of contact time on the adsorption of RB23+RB19 (a), RR23+$Fe^{3+}$ (b) and RB19+$Fe^{3+}$ (c) on the MCs/MS composite in the binary system (Bin). (Ambient temperature, Adsorbent mass=70 mg, Initial component concentration=50 mg/l, Stirring=150 rpm and pH~7)

Table 5. The equilibrium contact time for RR23, RB19 and $Fe^{3+}$ in single and binary systems of components. (Ambient temperature, Adsorbent mass=70 mg, Initial component concentration=50 mg/l, Stirring=150 rpm and pH~7)

| System | | Contact time in min | Qe in mg/g |
|---|---|---|---|
| **Single** | **RR23** | 180 | 18 |
| | **RB19** | 180 | 17.14 |
| | **$Fe^{3+}$** | 120 | 18 |
| **Binary** | **RR23+RB19** | | |
| | **RR23** | 180 | 9.3 |
| | **RB19** | 180 | 8.6 |
| | **RR23+$Fe^{3+}$** | | |
| | **RR23** | 120 | 10.65 |
| | **$Fe^{3+}$** | 180 | 10.67 |
| | **RB19+$Fe^{3+}$** | | |
| | **RB19** | 180 | 9.84 |
| | **$Fe^{3+}$** | 120 | 9.85 |

*3.3. The adsorption isotherm models applied to the multicomponent system*

To remove components from solutions, it's necessary to develop the adsorption system conception by using the best suitable correlation for the equilibrium curves. Divers models of isotherms have been used to demonstrate the experimental data of adsorption isotherms. The Langmuir model [30] is the most often used model, given

31

by equation (5), dimensionless constant called equilibrium parameter $R_L$ [31] represents the basic characteristic of Langmuir isotherm, which is specified by the equation (6).

$$q_e = Q_0 K_L C_e / (1 + K_L C_e) \quad (5)$$
$$R_L = 1/(1 + K_L C_e) \quad (6)$$

Where $q_e$, $C_e$, $Q_0$ and $K_L$ are the amount of solute adsorbed at equilibrium (mg/g), the concentration of adsorbate at equilibrium (mg/l), maximum adsorption capacity (mg/g) and Langmuir constant (L/mg), respectively. When $0 < R_L < 1$ the adsorption is effective, $R_L > 1$ the adsorption is equal to zero, $R_L = 0$ the adsorption is irreversible and $R_L = 1$ the representation of the isotherm is linear.

In this paper, a linear form of the expanded Langmuir model in the binary system of components 1 and 2 was used [32].

$$\left(C_{e,1} / q_{e,1}\right) = \left(1 / K_{L,1} Q_{0,1}\right) + \left(C_{e,1} / Q_{0,1}\right) + \left(q_{e,2} C_{e,1} / q_{e,1} Q_{0,2}\right) \quad (7)$$

The values of $(C_{e,1}/q_{e,1})$ had linear correlation with $(C_{e,1})$ and $(C_{e,1} q_{e,2}/q_{e,1}Q_{0,2})$ if the adsorption fallows the expanded Langmuir model. The isotherm parameters of an individual component in the binary system can be calculated by using the expanded Langmuir as a fit model.

The Freundlich model empirical equation is given by the linear form [33]:

$$LnQ_e = LnK_f + LnC_e/n_f \quad (8)$$

With $K_f$ is the relative adsorption capacity of the adsorbent and $n_f$ is the dependence degree of adsorption on the adsorbate equilibrium concentration.

Temkin model suppose that the adsorption energy of the molecules is reduced with the coverage ratio of the surface [32]. The Temkin isotherm linear transform is given by the equation (9):

$$q_e = B_1 \ln K_T + B_1 \ln C_e \quad (9)$$

Where
$$B_1 = RT / b$$

$K_T$ is the Temkin isotherm equilibrium binding constant (l/g), $B_1$ is the constant related to heat of sorption (J/mol), b is the Temkin isotherm constant, R and T are the universal gas constant (8.314 J/mol/K) and the absolute temperature (K), respectively.

The Dubinin-Radushkevich (DRK) isotherm [34] is usually applied to define the adsorption mechanism with a Gaussian energy distribution on a heterogeneous surface; the empirical form is given by the equation (10). The DRK isotherm constant $\varepsilon$ is given by the equation (11) This model used mostly to differentiate between physical and chemical adsorption of metal ions with its mean free energy E per molecule of adsorbate [35], calculated by the relation (12).

$$q_e = (q_s) \exp\left(-K_{ad} \varepsilon^2\right)$$
$$\ell n q_e = \ell n(q_s) - \left(K_{ad} \varepsilon^2\right) \quad (10)$$

$$\varepsilon = RT \ell n \left[1 + \frac{1}{C_e}\right] \quad (11)$$

$$E = \left[\frac{1}{\sqrt{2B_{DR}}}\right] \quad (12)$$

Where $q_e$ is the amount of adsorbate in the adsorbent at equilibrium (mg/g); $q_s$ is the theoretical isotherm saturation capacity (mg/g); $K_{ad}$ and $B_{DR}$ are the DRK isotherm constants $(mol^2/kJ^2)$ and $\varepsilon$ is the DRK isotherm constant. R, T and $C_e$ indicates the gas constant (8.314J/mol. K), absolute temperature (K) and adsorbate equilibrium concentration (mg/l), respectively.

The feasibility of Langmuir ($C_e/Q_e$ against $C_e$), Freundlich ($\ln Q_e$ versus $\ln C_e$) (Figures 11 and 12), Temkin ($Q_e$ versus $\ln C_e$) and Dubinin-Radushkevich ($\ln Q_e$ against $\varepsilon^2$) isotherms for the adsorption of components RR23, RB19 and $Fe^{3+}$ on the MCs/MS composite in single and binary systems are studied. The values of $Q_0$, $K_L$, $R_L$, $K_f$, $n_f$, $K_T$, $B_1$, b, $Q_s$, $K_{ad}$, E and $R^2$ (correlation coefficient values $R^2$ of all isotherms models) are shown in Table 6.
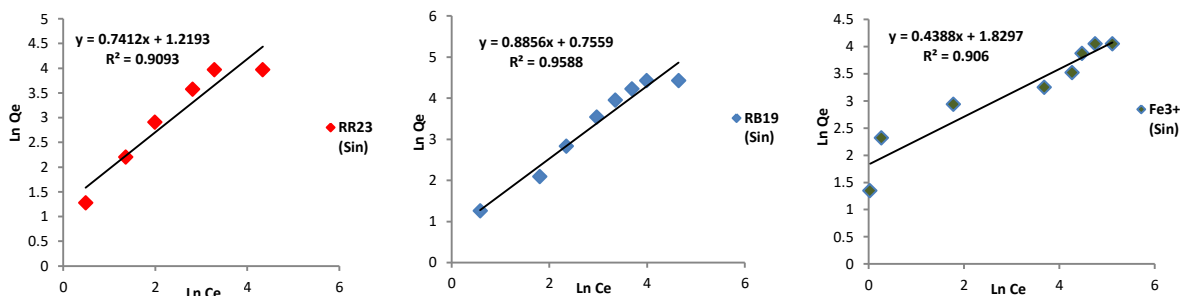
Figure 11. The Freundlich model for the adsorption of components RR23, RB19 and $Fe^{3+}$ on the MCs/MS composite in the single system (Sin). (Time=90 min, Ambient temperature, Adsorbent mass=70 mg, Stirring=150 rpm and pH~7)
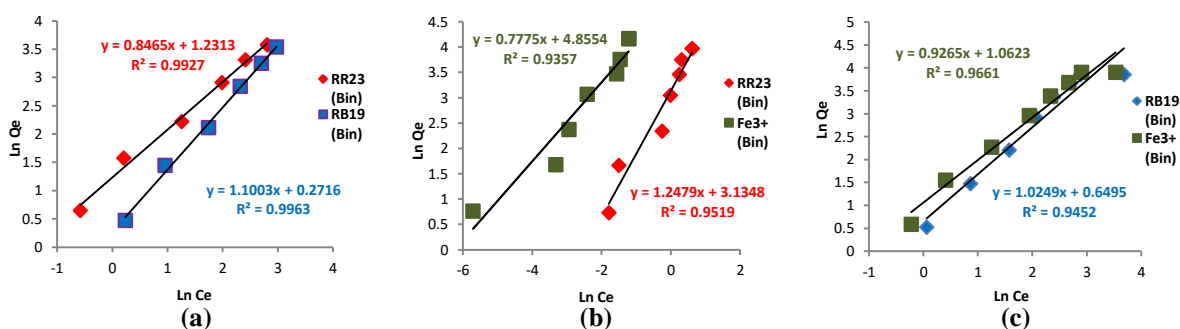


Figure 12. The Freundlich model for the adsorption of RR23+RB19 (a), RR23+$Fe^{3+}$ (b) and RB19+$Fe^{3+}$ (c) in the binary system (Bin) on the MCs/MS composite. (Time=90 min, Ambient temperature, Adsorbent mass=70 mg, Stirring=150rpm and pH~7)

According to Figures11 and 12 and all the results obtained in Table 6 we can notice that the Freundlich model represents the highest correlation coefficients ($R^2$) compared to the other models. The calculated correlation coefficients ($R^2$) for this isotherm model show that the adsorption isotherm of components RR23, RB19 and $Fe^{3+}$ on the MCs/MS composite in the single and binary systems follows the Freundlich isotherm as a fit model indicating that the adsorption is not limited to the formation of a monolayer with a non-uniform distribution of adsorption heat on the adsorbent surface.

Table 6. Adsorption isotherms constants of the components RR23, RB19 and $Fe^{3+}$ on the MCs/MS composite in single (Sin) and binary (Bin) systems. (Time=90 min, Ambient temperature, Adsorbent mass=70 mg, Stirring=150 rpm and pH~7)

| System | | Lungmuir Isotherm | | | | Freundlich Isotherm | | | Temkin Isotherm | | | | Dubinin-Radushkevich Isotherm | | | |
|---|---|---|---|---|---|---|---|---|---|---|---|---|---|---|---|---|
| | | $Q_0$ | $K_L$ | $R_L$ | $R^2$ | $K_f$ | $n_f$ | $R^2$ | $K_T$ | $B_1$ | $b$ | $R^2$ | $Q_s$ | $K_{ad}$ | $E$ | $R^2$ |
| Single | **RR 23** | | | | | | | | | | | | | | | |
| | | 71.942 | 0.045 | 0.224-0.9318 | 0.927 | 3.385 | 1.349 | 0.909 | 0.633 | 14.950 | 165.724 | 0.919 | 33.808 | 0.005 | 10.043 | 0.788 |
| | **RB19** | | | | | | | | | | | | | | | |
| | | 175.439 | 0.012 | 0.454-0.979 | 0.656 | 2.130 | 1.129 | 0.959 | 0.341 | 23.807 | 104.069 | 0.886 | 42.149 | 0.005 | 10.043 | 0.617 |
| | **$Fe^{3+}$** | | | | | | | | | | | | | | | |
| | | 62.112 | 0.040 | 0.132-0.96 | 0.890 | 6.232 | 2.279 | 0.906 | 1.388 | 9.443 | 262.369 | 0.870 | 38.394 | 0.007 | 8.279 | 0.848 |
| Binary | **RR23+RB19** | | | | | | | | | | | | | | | |
| | **RR23** | | | | | | | | | | | | | | | |
| | | 90.909 | 0.038 | 0.617-0.979 | 0.793 | 3.426 | 1.181 | 0.993 | 1.422 | 9.549 | 259.448 | 0.884 | 19.629 | 0.004 | 11.708 | 0.809 |
| | **RB19** | | | | | | | | | | | | | | | |
| | | 87.719 | 0.021 | 0.705-0.973 | 0.911 | 1.312 | 0.908 | 0.996 | 0.617 | 11.387 | 217.579 | 0.870 | 18.489 | 0.002 | 14.203 | 0.801 |
| | **RR23+$Fe^{3+}$** | | | | | | | | | | | | | | | |
| | **RR23** | | | | | | | | | | | | | | | |
| | | 50.251 | 0.285 | 0.653-0.954 | 0.480 | 22.984 | 0.801 | 0.952 | 4.923 | 19.818 | 125.016 | 0.793 | 40.169 | 0.001 | 23.416 | 0.895 |
| | **$Fe^{3+}$** | | | | | | | | | | | | | | | |
| | | 270.270 | 0.860 | 0.796-0997 | 0.077 | 128.432 | 1.286 | 0.936 | 114.730 | 13.410 | 184.756 | 0.682 | 47.546 | 0.000 | 38.607 | 0.809 |
| | **RB19+$Fe^{3+}$** | | | | | | | | | | | | | | | |
| | **RB19** | | | | | | | | | | | | | | | |
| | | 161.290 | 0.014 | 0.639-0.985 | 0.229 | 1.915 | 0.976 | 0.945 | 0.664 | 15.094 | 164.143 | 0.880 | 26.613 | 0.002 | 14.203 | 0.750 |
| | **$Fe^{3+}$** | | | | | | | | | | | | | | | |
| | | 121.951 | 0.026 | 0.528-0.979 | 0.589 | 2.893 | 1.079 | 0.966 | 0.915 | 14.437 | 171.613 | 0.909 | 29.374 | 0.007 | 8.279 | 0.815 |

### 3.4. The adsorption kinetic models applied to the multicomponent system

Several kinetic models are already used in literature to test the experimental data in order to undersdand the different mechanisms involved to master the adsorption process.

The pseudo first order model describing the phenomenon that occurred during the first minutes of the adsorption process. It is basically represented as follows [36]:

$$\frac{dq_t}{dt} = k_1(q_e - q_t) \tag{13}$$

After integration equation (13) by applying conditions, $q_t=0$ at $t=0$, we have:

$$q_t = q_e\left(1 - e^{-k_1 t}\right) \tag{14}$$

Linear form of the previous equation gives [37]:

$$\ln(q_e - q_t) = \ln q_e - k_1 t \tag{15}$$

Where $q_e$ is the component amount adsorbed at equilibrium (mg/g), $q_t$ is the component amount adsorbed at time t (mg/g) and $k_1$ is the equilibrium rate constant of pseudo first order kinetics (1/min) and t is the contact time (min). $k_1$ and $q_e$ are obtained from the line traced by $\ln(q_e - q_t) = f(t)$.

The pseudo second order model is applicable to a wider time interval mainly the entire adsorption process. It is given by the following expression [38]:

$$\frac{dq_t}{dt} = k_2(q_e - q_t)^2 \tag{16}$$

After the integration of equation (16), we obtain:

$$q_t = \left( \frac{k_2 q_e^2 t}{k_2 q_e t + 1} \right) \qquad (17)$$

The linearization of the preceding equation gives [23]:

$$\frac{t}{q_t} = \frac{1}{k_2 q_e^2} + \frac{1}{q_e} t \qquad (18)$$

Where $k_2$: the reaction speed constant of second order adsorption in (g/mg/min), $q_e$: the component amount adsorbed at equilibrium in (mg/g), $q_t$: the component amount adsorbed at time t (mg/g), t: contact time in (min). One traces $t/q_t = f(t)$, one obtains a line which gives $k_2$ and $q_e$.

Weber and Morris equation used to investigate the components molecules transporting possibility by the adsorbents particles. The intraparticle diffusion model [39] is given by the equation (19), this model contain a parameter C presenting the boundary layer thickness, the value of C gives an idea about the boundary layer thickness, as more the ordinate at the origin value is bigger, the effect of the boundary layer is more significant.

$$q_t = k_i t^{1/2} + C \qquad (19)$$

$q_t$ is the amount adsorbed at time t (mg/g), $K_i$ is the intraparticule diffusion constant (mg/g.min$^{1/2}$), t is contact time in (min) and C is the boundary layer thickness obtained by the intersection of the line with the Y-axis. The constant $K_i$ and the boundary layer thickness C are defined by tracing $q_t$ according to $t^{1/2}$.

The Elovich model is given by the following expression [40]:

$$\frac{dq_t}{dt} = \alpha \, exp(-\beta q_t) \qquad (20)$$

To linearize the Elovich equation it was assumed that $\alpha \, \beta \, t \gg 1$ and that $q_t = 0$ with t= 0, accordingly we obtained:

$$q_t = \frac{l}{\beta} \ln(\alpha\beta) + \ln(t) \qquad (21)$$

Where $\alpha$ and $\beta$ are the initial adsorption speed (mg/g.min) and the desorption constant (g/mg), respectively. Tracing $q_t = f(\ln t)$, the values of $\alpha$ and $\beta$ can be defined. Various kinetic models were studied such as the pseudo first order ($\ln(q_e - q_t)$ versus contact time t), pseudo second order ($t/q_t$ versus contact time t) Figures 13 et 14 , intraparticle diffusion ($q_t$ against $t^{1/2}$) and Elovich ($q_t$ versus $\ln(t)$) kinetic models. The different constants values of each model are shown in Table 7 such as $K_1$, $K_2$, $K_i$, C, $\beta$, $\alpha$ , $R^2$, $q_{e.exp}$, $q_{e.cal}$ ($R^2$ correlation coefficient values and $q_{e.exp}$, $q_{e.cal}$ for all kinetic models).From the finding of Figure 13, Figure 14 and Table 7, we notice that the pseudo second order model shows the highest correlation factor ($R^2$). We also see that the adsorption capacities calculated $(q_e)_{Cal}$ by this model are nearest to the experimental adsorption capacities $(q_e)_{Exp}$. Therefore the pseudo-second order model is the best fitting kinetic model for the adsorption process of components RR23, RB19 and $Fe^{3+}$ on the MCs/MS composite in both single (Sin) and binary (Bin) systems.
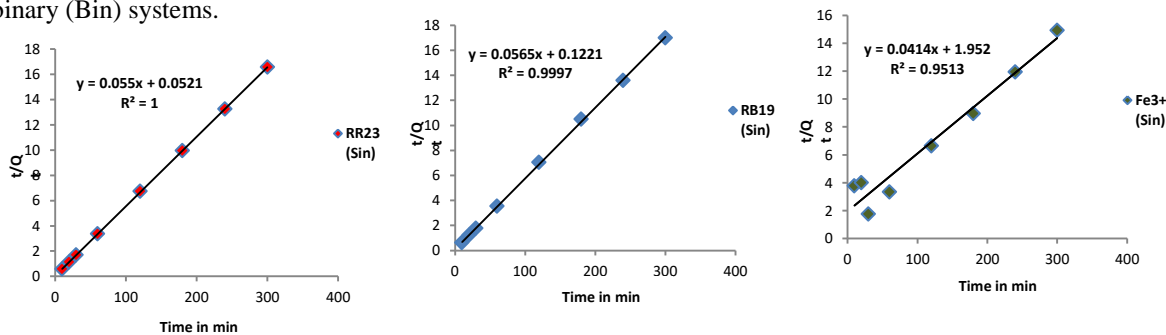


Figure 13. The pseudo second order kinetic model for the components RR23, RB19 and $Fe^{3+}$ adsorption on the MCs/MS composite in the single system (Sin). (Ambient temperature, Adsorbent mass=70 mg, Initial component concentration=50 mg/l, Stirring=150 rpm and pH~7)
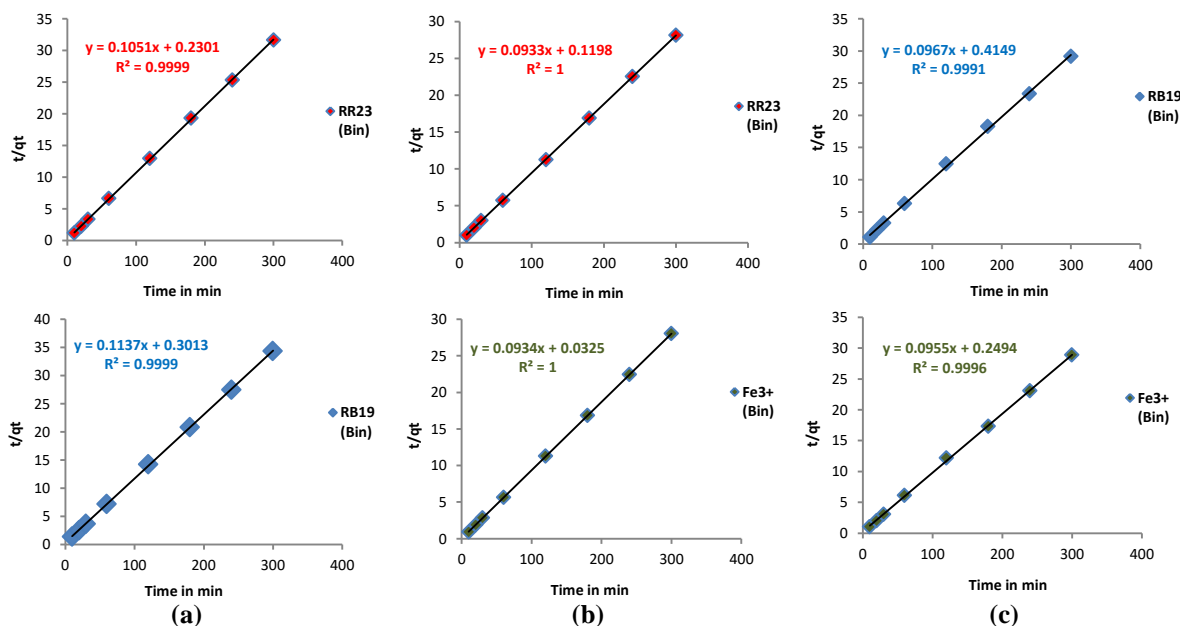
Figure 14. The pseudo second order kinetic model of the components adsorption RR23+RB19 (a), RR23+Fe$^{3+}$ (b) and RB19+Fe$^{3+}$ (c) in the binary system (Bin). (Ambient temperature, adsorbent mass=70 mg, Initial component concentration=50 mg/l, Stirring=150 rpm and pH~7)

Table 7. The adsorption kinetics constants of components RR23, RB19 and Fe$^{3+}$ on the MCs/MS composite in single (Sin) and binary (Bin) systems. (Ambient temperature, Adsorbent mass=70 mg, Initial component concentration=50 mg/l, Stirring=150 rpm and pH~7)

| System | | $(q_e)_{Exp}$ | Pseudo-first-order | | | Pseudo-second-order | | | Intraparticle diffusion | | | Elovich model | | |
|---|---|---|---|---|---|---|---|---|---|---|---|---|---|---|
| | | | $(q_e)_{Cal,}$ | $k_1$ | $R^2$ | $(q_e)_{Cal,}$ | $k_2$ | $R^2$ | $K_i$ | $C$ | $R^2$ | $\alpha$ | $\beta$ | $R^2$ |
| Single | RR23 | | | | | | | | | | | | | |
| | | 18.124 | 0.811 | 0.016 | 0.796 | 18.180 | 0.058 | 1.000 | 0.045 | 17.399 | 0.903 | $1.009364136 \times 10^{37}$ | 5.105 | 0.924 |
| | RB19 | | | | | | | | | | | | | |
| | | 17.675 | 1.033 | 0.004 | 0.823 | 17.699 | 0.026 | 1.000 | 0.077 | 16.321 | 0.911 | $4.585556874 \times 10^{20}$ | 3.102 | 0.878 |
| | Fe$^{3+}$ | | | | | | | | | | | | | |
| | | 20.090 | 21.482 | 0.034 | 0.836 | 24.155 | 0.001 | 0.951 | 1.051 | 4.887 | 0.621 | 1.493 | 0.201 | 0.767 |
| Binary | RR23+RB19 | | | | | | | | | | | | | |
| | RR23 | | | | | | | | | | | | | |
| | | 9.473 | 0.784 | 0.010 | 0.941 | 9.515 | 0.048 | 1.000 | 0.057 | 8.561 | 0.923 | $2.291815092 \times 10^{13}$ | 3.990 | 0.971 |
| | RB19 | | | | | | | | | | | | | |
| | | 8.732 | 1.027 | 0.013 | 0.861 | 8.795 | 0.043 | 1.000 | 0.080 | 7.520 | 0.719 | $2.60038767 \times 10^{7}$ | 2.687 | 0.854 |
| | RR23+Fe$^{3+}$ | | | | | | | | | | | | | |
| | RR23 | | | | | | | | | | | | | |
| | | 10.656 | 1.969 | 0.049 | 0.971 | 10.718 | 0.073 | 1.000 | 0.059 | 9.793 | 0.809 | $2.579514895 \times 10^{14}$ | 3.736 | 0.904 |
| | Fe$^{3+}$ | | | | | | | | | | | | | |
| | | 10.697 | 0.153 | 0.011 | 0.935 | 10.707 | 0.268 | 1.000 | 0.011 | 10.530 | 0.953 | $1.572966448 \times 10^{99}$ | 22.173 | 0.969 |
| | RB19+Fe$^{3+}$ | | | | | | | | | | | | | |
| | RB19 | | | | | | | | | | | | | |
| | | 10.285 | 1.228 | 0.006 | 0.954 | 10.341 | 0.023 | 0.999 | 0.088 | 8.767 | 0.963 | $1.62406853 \times 10^{9}$ | 2.749 | 0.900 |
| | Fe$^{3+}$ | | | | | | | | | | | | | |
| | | 10.393 | 0.694 | 0.002 | 0.656 | 10.471 | 0.037 | 1.000 | 0.058 | 9.443 | 0.876 | $9.507889377 \times 10^{15}$ | 4.246 | 0.804 |

*3.5. Effect of temperature and thermodynamic parameters:*

*3.5.1. Effect of temperature on the adsorption in multicomponent system*

The increase or decrease in temperature affects the adsorption capacity due to the following reasons: energy content, saturated vapor pressure and adsorbate density. Figures 15 and 16 illustrate the thermal agitation effect on the adsorption capacities of components RR23, RB19 and $Fe^{3+}$ in single and binary systems of components.
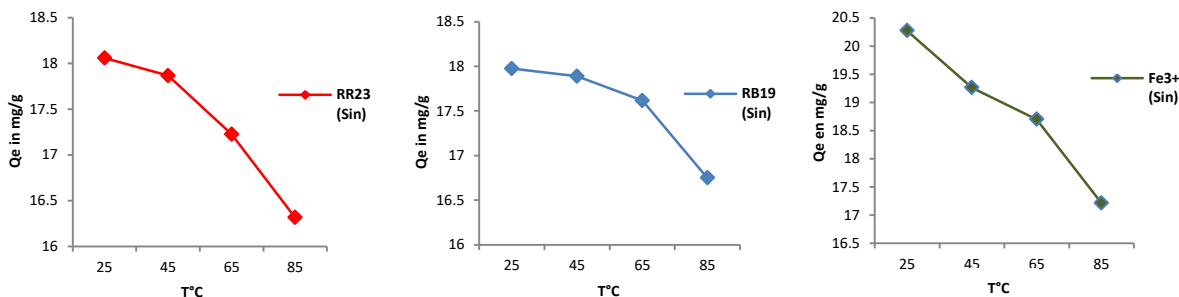


Figure 15. Effect of temperature on the adsorption of components RR23, RB19 and $Fe^{3+}$ on the MCs/MS composite in the single system (Sin). (Adsorbent mass=70 mg, Initial component concentration=50 mg/l, pH~7, Stirring=150 rpm)
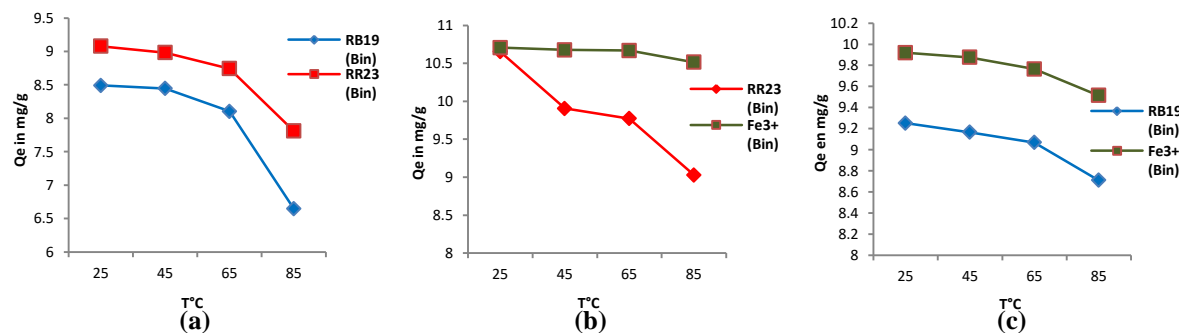


Figure 16. Effect of temperature on the adsorption of components RR23+RB19 (a), RR23+$Fe^{3+}$ (b) and RB19+$Fe^{3+}$ (c) on the MCs/MS composite in the binary system (Bin). (Adsorbent mass=70 mg, Initial component concentration=50 mg/l, pH~7, Stirring=150 rpm)

We can conclude from Figures 15 and 16 that the maximum adsorption capacity obtained at a temperature of 25 ℃ indicating that increasing the temperature decreases the adsorption capacities of components RR23, RB19 and $Fe^{3+}$ on the MCs/MS composite in both single (Sin) and binary (Bin) systems studied.

*3.5.2. Thermodynamic parameters in the multicomponent system*

To understand the matter transfer phenomena at the solid-liquid interface we must define thermodynamic parameters ΔG°, ΔH° and ΔS° by the path of the equation [41]:

$$Ln\ K_d = \Delta S°/R - \Delta H°/RT \qquad (22)$$

$$K_d = (C_0 - C_e)*V/(C_e*m) \qquad (23)$$

With ΔH° is the standard enthalpy (kJ/mol), ΔS° is the standard entropy (J/mol.K), T is the temperature in Kelvin, R is the gas constant (R=8.314 J/mol.K) and $K_d$ is the distribution coefficient calculated by the equation (23), $C_0$ is the initial component concentration in solution (mg/l), $C_e$ is the equilibrium concentration (mg/l), m is the adsorbent mass (g), V is the solution volume and $Q_e$ is the quantity adsorbed per unit adsorbent mass at equilibrium (mg/g). The values of the standard free enthalpy ΔG° (the free energy) of different components in both systems are obtained by the equation (24):

$$\Delta G° = - RTLnK_d \qquad (24)$$

Figures 17 and 18 illustrate the variation of $LnK_d$ as a function of $1/T$, from the trend curves we can define $\Delta H°$ and $\Delta S°$ for each component in both single and binary systems. The Table 8 summarizes all the thermodynamic parameters such as $\Delta H°$, $\Delta S°$ and $\Delta G°$ for all the components RR23, RB19 and $Fe^{3+}$ in single and binary systems.
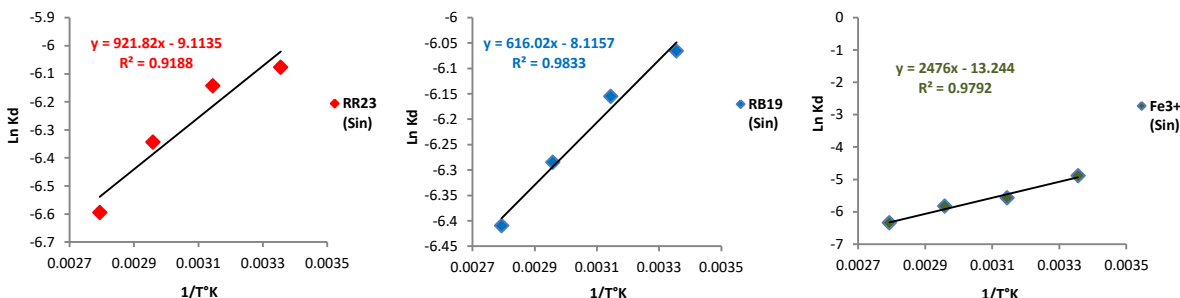


Figure17. Representation of $LnK_d$ as a function of $1/T$ for determining the thermodynamic parameters of components RR23, RB19 and $Fe^{3+}$ on the MCs/MS composite in the single system (Sin). (Adsorbent mass=70 mg, Initial component concentration=50 mg/l, pH~7, Stirring=150 rpm)
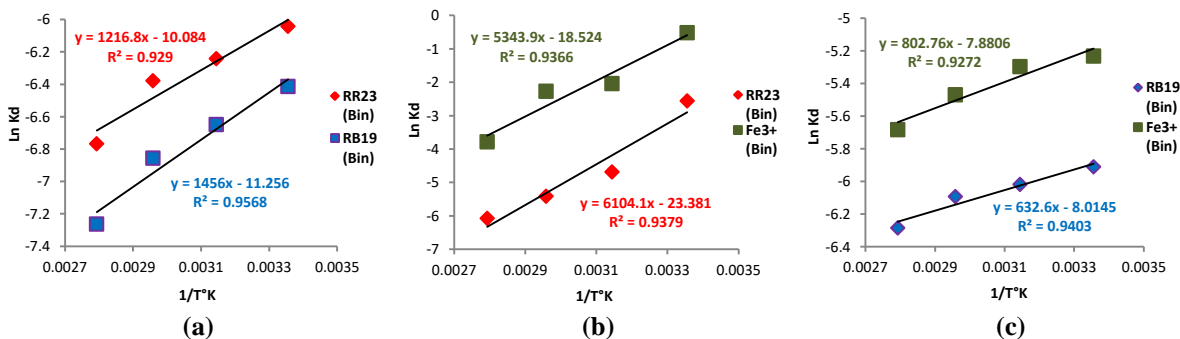


Figure 18. Representation of LnKd as a function of $1/T$ for determining the thermodynamic parameters of the components RR23+RB19 (a), RR23+$Fe^{3+}$ (b) and RB19+$Fe^{3+}$ (c) in the binary system (Bin). (Adsorbent mass=70 mg, Initial component concentration=50 mg/l, pH~7, Stirring=150 rpm)

From the results of Figures 17, 18 and Table 8 we can conclude that:

- $\Delta S°$ is negative for all the components in both systems proves that the adsorption is carried out with a rise in order at the solid-solution interface [42] and that the component molecules distribution order on the MCs/MS adsorbent is high compared with that in the solution.

- $\Delta G°$ rises up with rising the solution temperature which mean that the adsorption get very hard and disfavored by a higher temperature [43,44]. Energy redistribution between the adsorbent and the adsorbate [45] is quite clear because of $\Delta G°$ positive values, with an increase of the randomness at the solid-solution interface during the components fixing process RR23, RB19 and $Fe^{3+}$ on the MCs/MS composite in both single (Sin) and binary (Bin) systems, from these positive values of $\Delta G°$ we can say that the adsorption of the treated components is not spontaneous.

- $\Delta H°$ is negative for all the components in both single (sin) and binary (bin) systems which mean that our adsorption process is exothermic [42]. The chemisorption enthalpy is between 40 and 120 kJ/mol and for the physisorption it's less than 40kJ/mol [45]. The thermodynamic results found indicates that the nature of the adsorption is physical even whit the validity of the pseudo second order kinetics which introduce the probability of valence forces existence through sharing or exchange of electrons between the adsorbent and adsorbate. Both physical and chemical adsorption exist during the components fixation but the physisorption is more dominant due to the very low values of the standard enthalpy ($\Delta H°<40$ kJ/mol) [46,47].

Table 8. Thermodynamic parameters $\Delta H°$, $\Delta S°$ and $\Delta G°$ relating to the components RR23, RB19 and $Fe^{3+}$ adsorption on the MCs/MS composite in both single (Sin) and binary (Bin) systems. (Adsorbent mass=70 mg, Initial component concentration=50 mg/l, pH~7, Stirring=150 rpm)

| System | | $\Delta H°$ (kJ/mol) | $\Delta S°$ (J/mol.K) | $\Delta G°$ (kJ/mol) | | | |
|---|---|---|---|---|---|---|---|
| | | | | 298 K | 318 K | 338 K | 358 K |
| Single | RR23 | | | | | | |
| | | -7.664 | -75.770 | 15.056 | 16.242 | 17.829 | 19.629 |
| | RB19 | | | | | | |
| | | -5.122 | -67.474 | 15.127 | 16.220 | 17.493 | 19.286 |
| | $Fe^{3+}$ | | | | | | |
| | | -20.585 | -110.111 | 12.119 | 14.729 | 16.383 | 18.896 |
| Binary | RR23+RB19 | | | | | | |
| | RR23 | | | | | | |
| | | -10.116 | -83.838 | 14.970 | 16.501 | 17.922 | 20.140 |
| | RB19 | | | | | | |
| | | -12.105 | -93.582 | 15.892 | 17.579 | 19.268 | 21.621 |
| | RR23+$Fe^{3+}$ | | | | | | |
| | RR23 | | | | | | |
| | | -50.749 | -194.390 | 6.340 | 12.380 | 15.217 | 18.089 |
| | $Fe^{3+}$ | | | | | | |
| | | -44.429 | -154.009 | 1.284 | 5.400 | 6.387 | 11.269 |
| | RB19+$Fe^{3+}$ | | | | | | |
| | RB19 | | | | | | |
| | | -5.259 | -66.633 | 14.645 | 15.911 | 17.120 | 18.709 |
| | $Fe^{3+}$ | | | | | | |
| | | -6.674 | -65.519 | 12.966 | 14.007 | 15.374 | 16.920 |

## 4. Conclusion

Modified chitosan immobilized on modified sand (MCs/MS) bioadsorbent has demonstrated high efficiency in removing RR23, RB19 and $Fe^{3+}$ from wastewater in multicomponent systems, with a removal rate between 80% and 99% for all components in different systems. The amount of adsorbed components was higher in acidic medium (pH 1) due to the protonation of adsorbent active sites. The optimal initial components concentration to achieve the equilibrium adsorption capacity was 200mg/l for both single and binary systems with an optimal contact time between 120 min and 180 min. Removal of RR23, RB19 and $Fe^{3+}$ in multicomponent systems can be best described by the Freundlich model. Therefore, the pseudo second order model is the best fitting kinetic model for the adsorption process. The values of the thermodynamic parameters indicated that the adsorption of components is not spontaneous with an exothermic nature. The low enthalpy values confirm that the interaction between the adsorbent and the adsorbate is more prevailed by a physical adsorption. The present work revealed that our eco-friendly and low cost adsorbent MCs/MS is a promising material for the industrial wastewater treatment.

## References

[1] Gupta, V.K., Sharma, S. (2002), "Removal of cadmium and zinc from aqueous solutions using red mud", *Environmental Science & Technology* **36**(16), 3612–3617.

[2] Kieber, R.J., Williams, K., Willey, J.D., Skrabal, S., Avery, G.B. (2001), "Iron speciation in coastal rainwater: concentration and deposition to seawater", *Marine Chemistry* **73**(2), 83–95.

[3] Ngah, W. W., Ab Ghani, S., & Kamari, A. (2005), "Adsorption behaviour of Fe (II) and Fe (III) ions in aqueous solution on chitosan and cross-linked chitosan beads", *Bioresource Technology* **96**(4), 443-450.

[4] Dalida, M. L. P., Mariano, A. F. V., Futalan, C. M., Kan, C. C., Tsai, W. C., & Wan, M. W. (2011), "Adsorptive removal of Cu (II) from aqueous solutions using non-crosslinked and crosslinked chitosan-coated bentonite beads", *Desalination* **275**(1), 154-159.

[5] Pearce, C. I., Lloyd, J. R., & Guthrie, J. T. (2003), "The removal of colour from textile wastewater using whole bacterial cells: a review", *Dyes and Pigments* **58**(3), 179-196.

[6] McMullan, G., Meehan, C., Conneely, A., Kirby, N., Robinson, T., Nigam, P., Banat, I., Marchant, R., & Smyth, W. F. (2001), "Microbial decolourisation and degradation of textile dyes", *Applied Microbiology and Biotechnology* **56**(1), 81-87.

[7] Chiou, M.S., Ho, P.Y., Li, H.Y. (2004), "Adsorption of anionic dyes in acid solutions using chemically cross-linked chitosan beads"*, Dyes and Pigments* **60**(1), 69-84.

[8] Mohan, N., Balasubramanian, N., Basha C.A. (2007), "Electrochemical oxidation of textile wastewater and its reuse", *Journal of Hazardous Materials* **147**(1), 644-651.

[9] Sen, S., Demire, G.N. (2003), "Anaerobic treatment of real textile wastewater with a fluidized bed reactor", *Water Research* **37**(8), 1868-1878.

[10] Popuri, S. R., Vijaya, Y., Boddu, V. M., & Abburi, K. (2009), "Adsorptive removal of copper and nickel ions from water using chitosan coated PVC beads", *Bioresource Technology* **100**(1), 194-199.

[11] Dotto, G. L., Santos, J. M. N., Tanabe, E. H., Bertuol, D. A., Foletto, E. L., Lima, E. C., & Pavan, F. A. (2017), "Chitosan/polyamide nanofibers prepared by Forcespinning® technology: A new adsorbent to remove anionic dyes from aqueous solutions", *Journal of Cleaner Production* **144**,120–129.

[12] El Fargani, H., Lakhmiri, R., Albourine, A., Cherkaoui, O., Safi, M. (2016), "Valorization of shrimp co-products "Pandalus borealis": Chitosan production and its use in adsorption of industrial dyes", *Journal of Materials and Environmental Science* **7**(4), 1334-1346.

[13] Chen, A. H., Liu, S. C., Chen, C. Y., & Chen, C. Y. (2008), "Comparative adsorption of Cu (II), Zn (II), and Pb (II) ions in aqueous solution on the crosslinked chitosan with epichlorohydrin", *Journal of Hazardous Materials* **154**(1), 184-191.

[14] Ngah, W. W., & Fatinathan, S. (2008), "Adsorption of Cu (II) ions in aqueous solution using chitosan beads, chitosan–GLA beads and chitosan–alginate beads", *Chemical Engineering Journal* **143**(1), 62-72.

[15] Jeon, C., & Höll, W. H. (2003), "Chemical modification of chitosan and equilibrium study for mercury ion removal", *Water Research* **37**(19), 4770-4780.

[16] Ngah, W. W., Hanafiah, M. A. K. M., & Yong, S. S. (2008), "Adsorption of humic acid from aqueous solutions on crosslinked chitosan–epichlorohydrin beads: kinetics and isotherm studies", *Colloids and Surfaces B: Biointerfaces* **65**(1), 18-24.

[17] Kousalya, G. N., Gandhi, M. R., Sundaram, C. S., & Meenakshi, S. (2010), "Synthesis of nano-hydroxyapatite chitin/chitosan hybrid biocomposites for the removal of Fe (III)", *Carbohydrate Polymers* **82**(3), 594-599.

[18] Yadav, S., Srivastava, V., Banerjee, S., Weng, C. H., & Sharma, Y. C. (2013), "Adsorption characteristics of modified sand for the removal of hexavalent chromium ions from aqueous solutions: Kinetic, thermodynamic and equilibrium studies", *Catena* **100**, 120-127.

[19] Wan, M. W., Kan, C. C., Rogel, B. D., & Dalida, M. L. P. (2010), "Adsorption of copper (II) and lead (II) ions from aqueous solution on chitosan-coated sand", *Carbohydrate Polymers* **80**(3), 891-899.

[20] Wan, M. W., Petrisor, I. G., Lai, H. T., Kim, D., & Yen, T. F. (2004), "Copper adsorption through chitosan immobilized on sand to demonstrate the feasibility for in situ soil decontamination", *Carbohydrate Polymers* **55**(3), 249-254.

[21] Dalida, M. L. P., Mariano, A. F. V., Futalan, C. M., Kan, C. C., Tsai, W. C., & Wan, M. W. (2011), "Adsorptive removal of Cu (II) from aqueous solutions using non-crosslinked and crosslinked chitosan-coated bentonite beads", *Desalination* **275**(1), 154-159.

[22] Ngah, W. W., Ab Ghani, S., & Kamari, A. (2005), "Adsorption behaviour of Fe (II) and Fe (III) ions in aqueous solution on chitosan and cross-linked chitosan beads", *Bioresource Technology* **96**(4), 443-450.

[23] Mahmoodi, N. M., & Masrouri, O. (2015), "Cationic Dye Removal Ability from Multicomponent System by Magnetic Carbon Nanotubes", *Journal of Solution Chemistry* **44**(8), 1568-1583.

[24] Choy, K. K., Porter, J. F., & McKay, G. (2000), "Langmuir isotherm models applied to the multicomponent sorption of acid dyes from effluent onto activated carbon", *Journal of Chemical & Engineering Data* **45**(4), 575-584.

[25] Mahmoodi, N. M., Salehi, R., Arami, M., & Bahrami, H. (2011), "Dye removal from colored textile wastewater using chitosan in binary systems", *Desalination* **267**(1), 64-72.

[26] Saikia, B. J., Parthasarathy, G., & Sarmah, N. C. (2009), "fourier transform infrared spectroscopic characterization of Dergaon H5 chondrite: evidence of aliphatic organic compound", *Nature and Science* **7***(4)*, 45-51.

[27] Nyquist, R. A. (2001), "Interpreting infrared, Raman, and nuclear magnetic resonance spectra", *Academic Press*.

[28] Ioelovich, M. (2014), " Crystallinity and hydrophility of chitin and chitosan", *Journal of Chemistry* **3**(3), 7-14.

[29] Niu, C., Lu, Y. Z., & Lieber, C. M. (1993), "Experimental realization of the covalent solid carbon nitride", *Science* **261**(5119), 334-337.

[30] Langmuir, I. (1916), "THE CONSTITUTION AND FUNDAMENTAL PROPERTIES OF SOLIDS AND LIQUIDS. PART I. SOLIDS", *Journal of the American Chemical Society* **38**(11), 2221-2295.

[31] Das, S. K., Bhowal, J., Das, A. R., & Guha, A. K. (2006), "Adsorption behavior of rhodamine B on rhizopus o ryzae biomass", *Langmuir* **22**(17), 7265-7272.

[32] Allen, S. J., Mckay, G., & Porter, J. F. (2004), "Adsorption isotherm models for basic dye adsorption by peat in single and binary component systems", *Journal of colloid and interface science* **280**(2), 322-333.

[33] El Fargani, H., Lakhmiri, R., El Farissi, H., Albourine, A., Safi, M., Cherkaoui, O. (2017), "Removal of anionic dyes by silica-chitosan composite in single and binary systems: Valorization of shrimp co-product "Crangon-Crangon" and "Pandalus Borealis" ", *Journal of Materials and Environmental Science* **8**(2) 724-739.

[34] Dada, A. O., Olalekan, A. P., Olatunya, A. M., & Dada, O. (2012), "Langmuir, Freundlich, Temkin and Dubinin–Radushkevich isotherms studies of equilibrium sorption of Zn2+ unto phosphoric acid modified rice husk", *Journal of Applied Chemistry* **3**(1), 38-45.

[35] Dubinin, M. (1960), "The potential theory of adsorption of gases and vapors for adsorbents with energetically nonuniform surfaces", *Chemical Reviews* **60**(2), 235-241.

[36] Yuh-Shan, H. (2004), "Citation review of Lagergren kinetic rate equation on adsorption reactions", *Scientometrics* **59**(1), 171-177.

[37] BENAMROUI, F. (2015), "Élimination des colorants cationiques par des charbons actifs synthétisés à partir des résidus de l'agriculture", *PhD Thesis*.

[38] Ho, Y. S., & McKay, G. (1999), "Pseudo-second order model for sorption processes", *Process biochemistry* **34**(5), 451-465.

[39] Weber, W. J., & Morris, J. C. (1963), "Kinetics of adsorption on carbon from solution", *Journal of the Sanitary Engineering Division* **89**(2), 31-60.

[40] Lv, L., He, J., Wei, M., Evans, D. G., & Duan, X. (2006), "Uptake of chloride ion from aqueous solution by calcined layered double hydroxides: equilibrium and kinetic studies", *Water Research* **40**(4), 735-743.

[41] Laabd, M., El Jaouhari, A., Bazzaoui, M., Albourine, A., Lakhmiri, R. (2014), "Removal of Polycarboxylic Benzoic Acids by Adsorption onto Polyaniline-Polypyrrole from Aqueous Solution", *International Journal of Engineering Research and Technology* **3**(11).

[42] Aarfane, A., Salhi, A., El Krati, M., Tahiri S., Monkade, M., Lhadi, E .K., Bensitel M. (2014), "Etude cinétique et thermodynamique de l'adsorption des colorants Red195 et Bleu de méthylène en milieu aqueux sur les cendres volantes et les mâchefers (Kinetic and thermodynamic study of the adsorption of Red195 and Methylene blue dyes on fly ash and bottom ash in aqueous medium) ", *Journal of Materials and Environmental Science* **5**(6), 1927-1939.

[43] Talidi, A. (2006), "Etude de l'élimination du Chrome et du bleu de méthylène en milieux aqueux par adsorption sur la pyrophyllite traitée et non traitée", *PhD Thesis*.

[44] Namasivayam, C., Senthilkumar, S. (1998), "Removal of arsenic (V) from aqueous solution using industrial solid waste: adsorption rates and equilibrium studies", *Industrial & Engineering Chemistry Research* **37**(12), 4816-4822.

[45] Gherbi, N. (2008), "Etude expérimentale et identification du processus de rétention des cations métalliques par des matériaux naturels", *PhD Thesis*, Université de Constantine pp.

[46] Ahmad, R., Kumar, R. (2010), "Adsorptive removal of congo red dye from aqueous solution using bael shell carbon", *Applied Surface Science* **257**(5), 1628-1633.

[47] Zhang, Z., O'Hara, I. M., Kent, G. A., Doherty, W. O. (2013), "Comparative study on adsorption of two cationic dyes by milled sugarcane bagasse", *Industrial Crops and Products* **42,** 41-49.